# Clear-Sky Bidirectional Reflectance Functions Derived from ARM-UAV MPIR and CERES Helicopter Data Over the ARM SGP Site

*S. Mayor and D. R. Doelling*
*Analytical Services and Materials, Inc.*
*Hampton, Virginia*

*P. Minnis and D. R. Cahoon*
*National Aeronautics and Space Administration*
*Langley Research Center*
*Hampton, Virginia*

*G. S. Phipps*
*Sandia National Laboratories*
*Albuquerque, New Mexico*

## Introduction

Bidirectional reflectance distribution functions (BRDFs) are essential for deriving albedos from radiances measured by satellites to estimate the observed global energy balance and for predicting the radiance field for a given set of conditions. Data taken by the high-resolution Multispectral Pushbroom Imaging Radiometer (MPIR) on the Atmospheric Radiation Measurement-Unmanned Aerospace Vehicle (ARM-UAV) during the Fall 1996 Flight Series are used to derive a set of visible channel clear-sky BRDFs. BRDFs were also derived from data taken by the helicopter-based Clouds and the Earth's Radiant Energy System (CERES) Airborne Radiometer Scanner (ARS; Wheeler et al. 1997) system over a variety of surface types around the ARM Southern Great Plains (SGP) site during August 1998. The BRDFs were computed using clear-sky data in spectral intervals corresponding to channels on several new satellite imagers. The results are compared for variability with wavelength and surface type. The reflectances were corrected to the top of the atmosphere (TOA) for use with satellite data. These results should help improve the accuracy of satellite-derived cloud and surface radiative properties.

## Data

The MPIR was built and fielded by Sandia National Laboratories, Albuquerque, New Mexico, to provide quantitative radiance data in nine spectral bands. The instrument was mounted downlooking on the UAV during the Fall 1996 Intensive Observation Period (IOP) with an 11° tilt to port. The cross-track field-of-view is ±40°. The surface resolution is ~0.1 km at a UAV altitude of 15 km. Only high resolution channel-1 (645 nm) data from 3 days (September 29, October 3, and October 5, 1996) were used in this study to derive visible channel clear-sky BRDFs. Data from these flights were taken at

altitudes between 6 km and 12 km at viewing zenith angles (VZAs) between 0° and 60° because of the limited cant of the MPIR on the UAV. Most flights occurred near noon (SZA ~45°) but data from one 24-hour flight covered higher solar zenith angles (SZA = 53° to 90°).

The CERES ARS system consists of a self-navigating Bell UH-1H helicopter-based scanner system, which allows precise measurement of surface BRDFs. The FieldSpec FR spectroradiometer, built by Analytical Spectral Devices provides nearly continuous spectral sampling from 0.35 μm to 2.5 μm in 3-nm to 12-nm intervals. During bidirectional operations, the starboard pod (containing the FieldSpec FR) rotates along the pitch plane in order to track ground targets as shown in Figure 1.

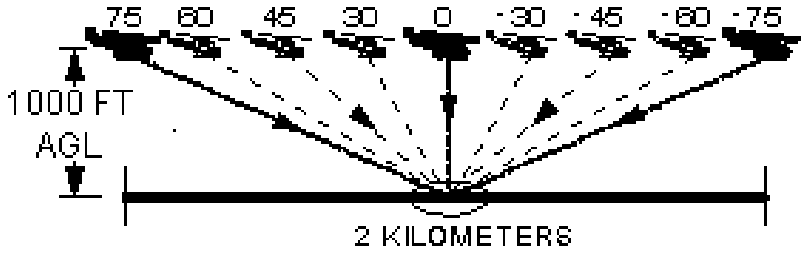


**Figure 1**. Vertical flight-leg profile for helicopter flight pattern.

As the ARS passes over the ground target, the starboard pod maintains a constant fix, thus providing continuous measurements from +75° to -75° relative to nadir. Five leg patterns are flown, as shown in Figure 2, to allow ten separate azimuthal measurements over the target. Bidirectional measurements have been taken over a variety of vegetation types (e.g., fallow wheat, grass, milo, and soybeans) around the SGP Cloud and Radiation Testbed (CART) site.

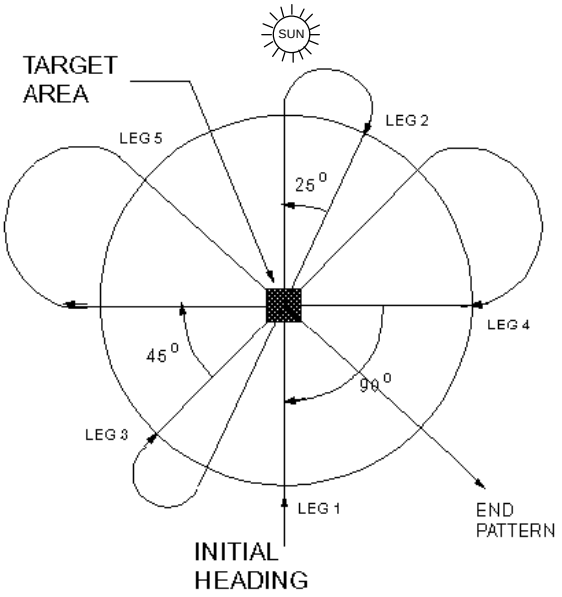


**Figure 2**. CERES ARS typical BRDF pattern (overhead view).

## Methodology

To describe the angular variation of radiance, the angular coordinates were divided into ranges called "bins," and the model was represented by mean values for each bin. For MPIR, these bins were defined by increments of 10° VZA, 15° relative azimuth angle (except the first two and last two bins were 7.5°), and 10° SZA. Data from all 3 days were averaged into these bins. For the helicopter, these bins are defined by increments of 10° VZA, 10° SZA and, relative azimuths centered at 6°, 25°, 45°, 90°, 135°, 155°, and 174°. Data from all vegetation types were averaged into these bins.

Because the albedo of land surfaces, especially bare soil, varies as a function of surface dampness, the 3 days were evaluated for wet/dry conditions. A plot of the diurnal variation of albedo in the 0.5° box around the SGP CART site from Geostationary Operational Environmental Satellite (GOES)-8 (Figure 3) showed a significantly lower albedo for September 29 compared to October 3, indicating the ground was still wet from rains that occurred on September 26. Thus, MPIR reflectances from September 29 were normalized to the October 3 albedo from GOES.

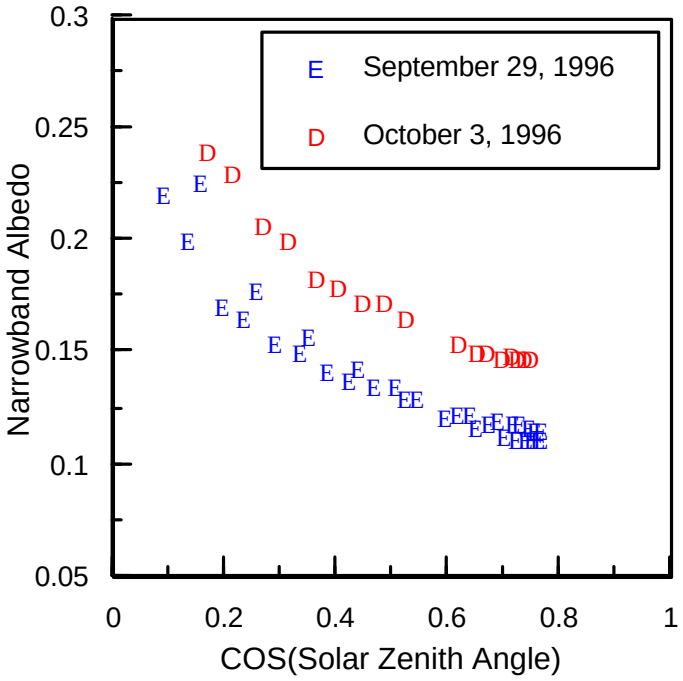


**Figure 3**. Clear-sky narrowband visible albedos derived from GOES-8 for a 0.5° box centered at the central facility.

To apply the model to satellite data, the reflectances were corrected to the TOA by accounting for molecular scattering and ozone absorption. For this analysis, all aerosols were assumed to be below the UAV. The correction for ozone absorption and Rayleigh scattering follow the procedures of Minnis et al. (1993). The reflectance parameterization for MPIR is described below. A similar parameterization was applied to the helicopter data.

The reflectance at the TOA is

$$p_{TOA} = t_{\mu}\left[p_{ray}(\mu_o, \mu, \psi) + p_{mpir}(\mu_o, \mu, \psi)\right] \quad (1)$$

where $t_{\mu}$ is the upward transmittance and $\rho_{ray}$ is the reflectance of overlying Rayleigh layer. The reflectance at the MPIR, $\rho_{mpir}$, is defined as

$$p_{mpir} = \frac{R_{meas}}{E\lambda\left(1-\alpha_{ray}\right)_{\tau_{a1}}} \quad (2)$$

where $\alpha_{ray}$ is the albedo of Rayleigh layer above the UAV, $E\lambda$ is the spectral solar constant (value used in this analysis for MPIR channel 1 is 73.88 $Wm^{-2}$ and for helicopter visible channel is 1442.27 $Wm^{-2}\mu m^{-1}$), $R_{meas}$ is the radiance measurement at flight level, $t_{a1}$ is the transmittance of ozone above the UAV, $\mu$ is cos(SZA), $\mu_o$ is cos(VZA), and the relative azimuth angle is $\Psi$. For this analysis, the ozone absorption optical depth for the visible channel is fixed at 0.027, a value that corresponds to an ozone path length of 0.35 cm-STP.

Due to the limited flight patterns, the time of year and the latitude, not all VZA and SZA bins were filled for the two channels. The most serious problem was values missing for entire SZA bins. To fill some of the empty bins, the Helmholtz Principle of Reciprocity,

$$\mu_o L(\mu_o, \psi; \mu) = (\mu, \psi; \mu_o)$$

was applied first. For reciprocal bins with data derived from MPIR, the difference between the observed and predicted radiances (Figure 4) is unbiased with a root mean square (rms) difference of 15.8%, indicating that the use of this principle here is justified. Similar results were obtained for helicopter data. Much of the scatter may be due to the variations in the observed scenes.

To complete the MPIR model, the radiances missing at low VZA bins for low SZAs were predicted from radiances in bins with data and corrected with the narrowband BRDFs of Minnis and Harrison (1984; MH). Similarly, Earth Radiation Budget Experiment (ERBE) BRDFs (Suttles et al. 1988) were used with the filled bins to fill empty high VZA bins at high SZAs.

To complete each helicopter model, the missing radiances were filled using extrapolation (second degree polynomial fits) and interpolation techniques.

The corrected radiances in the angular bins were then combined using pixel-weighted averages.

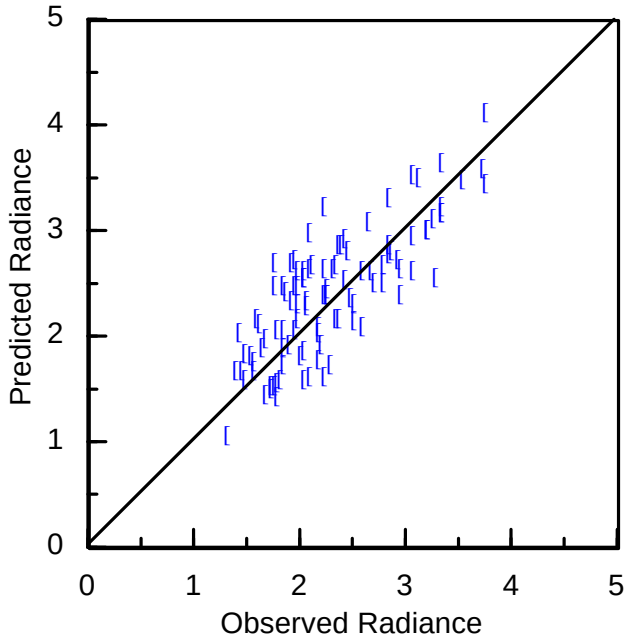


**Figure 4**. Application of reciprocity to filled angular bins yielded an rms of 15.8% with bias = -0.0054 (Radiance is in $Wm^{-2}sr^{-1}$).

## Results

The MPIR and helicopter data were used to generate reflectances at the instrument altitude and at the TOA. Next, the reflectances were computed at the TOA by applying Eqs. (1) and (2). These corrections increased the reflectances by about 20%. Finally, the TOA reflectances were integrated over all angles and normalized to create the BRDF models.

In general, the anisotropic factors have small variations over the first three SZA bins (not shown), but significant increases in the forward and back scattering peaks are observed at higher SZAs. Figures 5 and 6 compare the MPIR-derived and helicopter-derived BRDF's with the MH BRDFs for SZA of 55°, respectively. The major features of the two models are similar. Overall, the MPIR and helicopter BRDFs show more structure than the MH models. The MH models are most likely smoother because they are derived from low-level aircraft data taken over a wide variety of land regions while the MPIR and helicopter data were limited to the ARM SGP region and contain estimates for some bins. The MH models were not corrected to the TOA. All three models become more anisotropic with increasing SZA. The models also show a strong backscattering peak near the anti-solar point and a minimum near nadir in the forward scattering direction.

The BRDF models will be tested using simultaneous visible channel observations from multiple GOES and sun-synchronous satellites. Reflectance from a scene observed by one satellite is used with the BRDF model to predict the reflectance for the other satellite. This approach to estimating the model errors is currently under way.

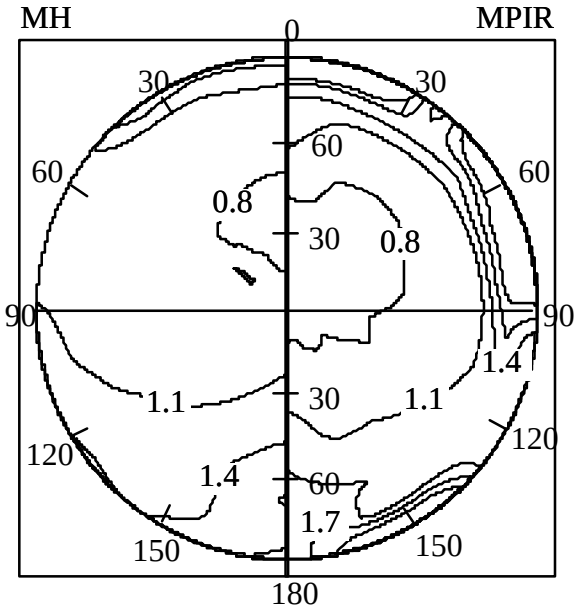


**Figure 5**. Comparison of anisotropic visible reflectance factors derived from ARM-UAV MPIR measurements over SGP and MH BRDF (SZA = 55°).

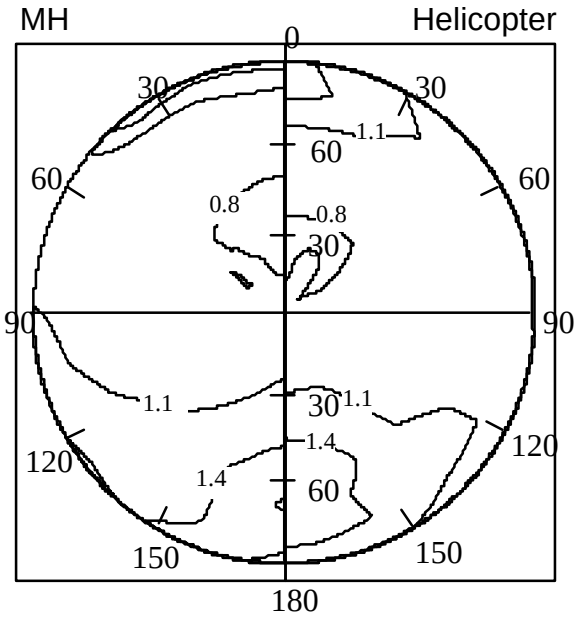


**Figure 6**. Comparison of anisotropic visible reflectance factors derived from helicopter measurements (0.65 μm) at TOA over SGP and MH BRDF (SZA = 55°).

## Concluding Remarks

The MPIR and helicopter-derived BRDF models should improve accuracy of ARM satellite-derived cloud and radiation products because they are specifically representative of the SGP area. Despite limited coverage, the major features of the models compared reasonably well with the MH and ERBE BRDFs. Because of its high ceiling, the UAV/MPIR can provide BRDFs useful for satellite interpretation without relying on models to account for aerosol and atmospheric scattering. Inclusion of aerosols in the correction atmospheric effects of the helicopter data should improve the accuracy of resulting TOA BRDFs. Filling missing angular bins increased uncertainty in the derived BRDF model. Hence, data from additional clear-sky UAV and helicopter flights are needed to fill more bins and reduce dependence on auxiliary bin filling techniques.

## Acknowledgments

This research was supported by DE-AI02-97ER62341 as part of the ARM Science Team and by the National Aeronautics and Space Administration (NASA) CERES Project. The helicopter data were provided by Bob Wheeler of Analytical Systems and Materials, Inc. Sean Moore of Mission Research Corporation, Santa Barbara, California, provided assistance in the development of software to geolocate the MPIR radiances.

# References

Minnis, P., and E. F. Harrison, 1984: Diurnal variability of regional cloud and clear-sky radiative parameters derived from GOES data; Part I: Analysis method. *J. Climate Appl. Meteor.*, **23**, 993-1011.

Minnis, P., K. Liou, and Y. Takano, 1993: Inference of cirrus cloud properties using satellite-observed visible and infrared radiances. I - Parameterization of radiance fields. *J. Atmos. Sci.*, **50**, 1279-1304.

Suttles, J. T., R. N. Green, P. Minnis, G. L. Smith, W. F. Staylor, B. A. Wielicki, I. J. Walker, D. F. Young, V. R. Taylor, and L. L. Stowe, 1988: Angular radiation models for earth-atmosphere system, Vol. I, Shortwave radiation. *NASA Ref. Publ., 1184*.

Wheeler, R. J., G. C. Purgold, and C. H. Whitlock, 1997: The CERES airborne radiometer scanner. *9th Conference on Atmospheric Radiation*, 2-7 February, Long Beach, California.